www.sciencemag.org/cgi/content/full/science.1248213/DC1

Supplementary Materials for

Order of Magnitude Smaller Limit on the Electric Dipole Moment of the Electron

The ACME Collaboration,* J. Baron, W. C. Campbell, D. DeMille,† J. M. Doyle,† G. Gabrielse,† Y. V. Gurevich, P. W. Hess, N. R. Hutzler, E. Kirilov, I. Kozyryev, B. R. O'Leary, C. D. Panda, M. F. Parsons, E. S. Petrik, B. Spaun, A. C. Vutha, A. D. West

*The collaboration consists of all listed authors. There are no additional collaborators.
†Corresponding author. E-mail: acme@physics.harvard.edu (D.D., J.M.D., G.G.)

Published 19 December 2013 on *Science* Express
DOI: 10.1126/science.1248213

This PDF file includes:

Materials and Methods

Fig. S1

Table S1

References

Supplementary Materials

Apparatus

We create a pulsed molecular beam of ThO using the buffer gas beam technique[16–18]. Each packet of molecules leaving the source contains $\sim 10^{11}$ ThO molecules in the $J = 1$ rotational level of the ground electronic (X) and vibrational state and are produced at a repetition rate of 50 Hz. The packet is 2-3 ms wide and has a center of mass speed of ~ 200 m/s. The chamber background pressure of $< 10^{-6}$ Torr suggests a ThO-background gas collision probability of $\lesssim 1\%$ during the spin precession measurement which could cause a small decrease in fluorescence signal or contrast.

After leaving the cryogenic beam source chamber, the ground state molecules are in a thermal distribution of rotational states at about 4 K with a rotational constant of about $B_{\rm R} \approx 10$ GHz. We use a series of lasers and microwaves to enhance the population of the single rotational state, $|X; J = 1\rangle$. The molecules travel through optical pumping lasers resonant with the $|X; J = 2, 3\rangle \rightarrow |C; J = 1, 2\rangle$ transitions, followed by a microwave field resonant with the $|X; J = 0\rangle \leftrightarrow |X; J = 1\rangle$ transition. The optical pumping lasers transfer population from $|X; J = 2, 3\rangle$ into the $|X; J = 0, 1\rangle$ states respectively. The microwaves then mix the populations of $|X; J = 0, M = 0\rangle$ and $|X; J = 1, M = 0\rangle$ resulting in an overall population increase in $|X; J = 1\rangle$ of a factor of ~ 2.

The molecules then pass through adjustable and fixed collimating apertures before entering the magnetically shielded interaction region, where electric and magnetic fields are applied. The quantization axis is not preserved between the microwave region and the electric field plates so the population in the three M sublevels of $|X; J = 1\rangle$ are mixed. A retroreflected 943 nm laser optically pumps population from the $|X; J = 1, M = \pm 1\rangle$ states to $|A; J = 0, M = 0\rangle$, which spontaneously decays partially into the $|H; J = 1\rangle$ state in which the EDM measurement is performed.

The spin precession region contains applied electric and magnetic fields, along with lasers to prepare and read our EDM state. The electric field is provided by two plates of 12.7 mm thick glass coated with a layer of indium tin oxide (ITO) on one side, and an anti-reflection coating on the other. The ITO coated sides of the plates face each other with a gap of 25 mm, and a voltage is applied to the ITO to create a uniform electric field.

The spatial profile of the electric field was measured by performing microwave spectroscopy on the ThO molecules. When the molecule pulse is between the state preparation and read-out regions, a 40 µs burst of microwaves resonant with the DC Stark-shifted $|H; J = 1, M = \pm 1\rangle \rightarrow |H; J = 2, M = 0\rangle$ transitions is introduced by a microwave horn at the end of the apparatus, counterpropagating to the molecular beam. If on resonance, the microwaves drive a transition that spin-polarizes the molecules, similar to the state preparation scheme. We can then detect the spin polarization using the normal readout scheme. The microwave transition width is ~ 5 kHz (dominated by Doppler broadening), so the H-state dipole moment of $D \approx 1$ MHz/(V/cm)[11] (for $J = 1$) means that this method is sensitive to mV/cm electric field deviations with spatial resolution of 1 cm, limited by the velocity distribution in the beam. Our measurement indicated that the spatial variation of the electric field plate separation is ~ 20 µm across the molecule precession region, in very good agreement with an interferometric measurement[32]. We can also test how well the electric field reverses by mapping the field with equal and opposite voltages on the plates. This measurement indicated that the non-reversing component of the electric field had magnitude $|\mathcal{E}^{\rm nr}| \approx$ 1-5 mV/cm across the entire molecular precession region, as shown in Figure 3B.

The EDM measurement is performed in a vacuum chamber surrounded by five layers of mu-metal shielding. The applied magnetic field is supplied by a cosine-theta coil, with several shim coils to create a more uniform magnetic field within the precession region, and to allow us to apply transverse magnetic fields and gradients for systematic checks. Changes in the magnetic field are monitored by four 3-axis fluxgate magnetometers inside the magnetic shields, and the magnetic fields were mapped out before and after the experimental dataset was taken by sliding a 3-axis fluxgate down the beamline.

The lasers travel through the electric field plates, so all stages of the spin precession measurement are performed inside the uniform electric field. All laser light in the experiment originates from external cavity diode lasers (ECDL), frequency stabilized via an Invar transfer cavity to a CW Nd:YAG laser locked to a molecular iodine transition[33]. All required transition frequencies and state assignments were determined previously[34–36]. We measured the saturation intensities, radiative lifetimes, electric/magnetic dipole moments, and branching ratios for all required states and transitions.

In order to normalize against drifting molecular beam properties (pulse shape, total molecule number, velocity mean and distribution, etc.), we perform a spin precession measurement every 10 µs, which is much faster than the molecular beam variations[15], spin precession time, and temporal width of the molecular pulse. The ~ 20 µs fly-through interaction time with the readout laser allows each molecule to be read-out by both $\hat{X}$ and $\hat{Y}$ polarizations. This is accomplished by sending the detection laser through two different beam paths, combined on the two ports of a polarizing beamsplitter. The two beam paths can be rapidly switched on and off with acousto-optic modulators (AOMs). The maximum rate of the polarization switching is limited by the 500 ns lifetime of the C state (decay rate of $\gamma \approx 2\pi \cdot 0.3$ MHz). A 1.2 µs delay is inserted between the pulses of $\hat{X}$ and $\hat{Y}$ polarized readout light (Fig. S1A), which minimizes the amount of residual fluorescence overlapping between subsequent polarization states. Since the polarization switching period is longer than the decay time of the C state, we expect $\lesssim 1$ percent of the C state population to spontaneously decay back to the H state while the molecules are in the readout laser beam. Each of these two effects reduces the contrast by about 1 percent. We searched for, but did not observe, changes in $\omega^{\mathcal{NE}}$ as a function of time within a polarization cycle.

The transparent electric field plates allow us to collect a large fraction of the solid angle of fluorescence from the molecules. Fluorescence travels through the field plates into an eight-lens system (four behind each plate) which focuses the light into an optical fiber bundle. The four bundles on each side are coupled into a fused quartz light pipe, which carries the fluorescence to a PMT (outside the magnetic shields). The net detection efficiency, including collection solid angle and detector quantum efficiency, is about 1%. We typically register around 1000 photon counts per molecule pulse (Fig. S1B). The PMT photocurrents are read as analog signals by a low-noise, high-bandwidth amplifier, and then sent to a 24-bit digitizer operating at 5 megasamples/s. The control and timing for all experimental parameters is managed by a single computer, and the timing jitter is less than one digitizer sampling period.

Systematic Errors

The presence of a nonzero magnetic field component $\mathcal{B}_z$ (parallel or antiparallel to the electric field), leads to a nonzero two photon detuning, $\delta = 2\mu_B g\tilde{\mathcal{B}}\,|\mathcal{B}_z|$, for the Λ system characterized

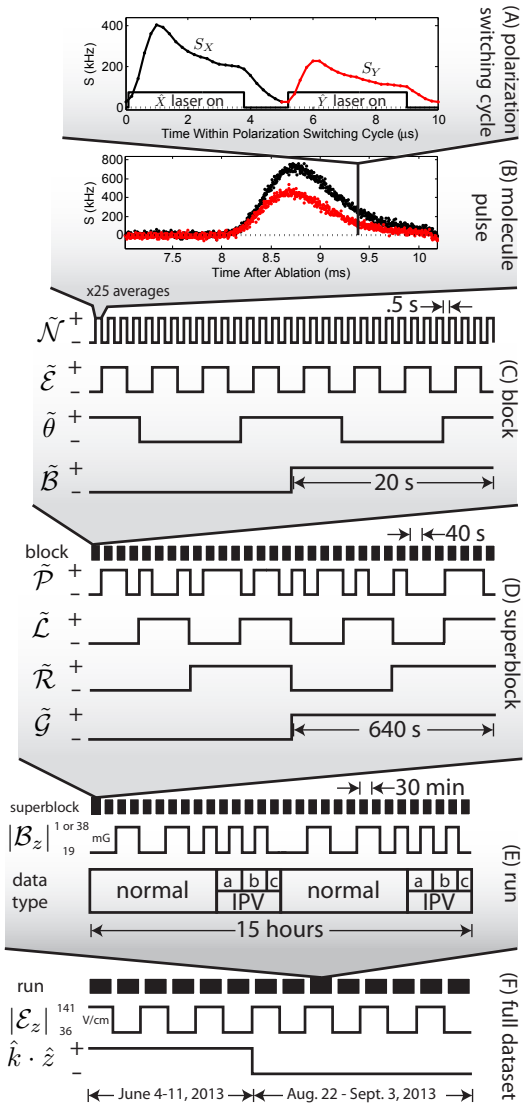

FIG. S1. **Relevant switching timescales (A)** Time within the readout laser polarization switching cycle with a period of 10 μs. The molecule fluorescence rises rapidly when the laser is switched on, decays with rate $\gamma/2$ to a steady state (due to additional molecules entering the laser beam), and then decays with rate γ after the laser is switched off. Fluorescence is measured in detected photoelectrons/ms (kHz). **(B)** Time within the ThO molecule pulse after its creation by laser ablation. The fluorescence signals from (A) have been split up according to readout laser polarization to obtain the plotted points labeled by S_X and S_Y. The displayed fluorescence traces are averaged over 400 pulses, but 25 pulses are averaged for a given state of the experiment. **(C)** Switches performed within a block of data. The $\tilde{\mathcal{N}}$ switch randomly alternates between a $(-+)$ and $(+-)$ pattern, the $\tilde{\mathcal{E}}$ and $\tilde{\theta}$ switches randomly alternate between a $(-++-)$ and $(+--+)$ pattern, and the $\tilde{\mathcal{B}}$ switch alternates between a $(-+)$ and $(+-)$ pattern between blocks. **(D)** Switches performed within a superblock of data. The $\tilde{\mathcal{P}}$ state is assigned randomly between blocks, but other superblock patterns are deterministic. **(E)** Changes in the experimental procedure between superblocks. We alternated between taking data under "normal" conditions and taking data with "intentional parameter variations" (IPV), which were used to monitor systematic effects. The IPVs are a=$\mathcal{E}^{\rm nr}$, b=$\Omega_{\rm r}^{\mathcal{NE}}$, and c=$\Delta_{\rm prep}$ (which was used to monitor the value of $\mathcal{E}^{\rm nr}$ by exaggerating its effect on the $\tilde{\mathcal{N}}\tilde{\mathcal{E}}$ correlated contrast). **(F)** An overview of the ~ 2 weeks of data comprising our reported EDM measurement.

Category I Parameters
Magnetic Fields
- Non-Reversing $\mathcal{B}$-Field: $\mathcal{B}_z^{\rm nr}$
- Transverse $\mathcal{B}$-Fields: $\mathcal{B}_x, \mathcal{B}_y$ (even and odd under $\tilde{\mathcal{B}}$)
- Magnetic $\mathcal{B}$-Field Gradients: $\frac{\partial \mathcal{B}_x}{\partial x}, \frac{\partial \mathcal{B}_y}{\partial x}, \frac{\partial \mathcal{B}_y}{\partial y}, \frac{\partial \mathcal{B}_y}{\partial z}, \frac{\partial \mathcal{B}_z}{\partial x}, \frac{\partial \mathcal{B}_z}{\partial z}$ (even and odd under $\tilde{\mathcal{B}}$)
- $\tilde{\mathcal{E}}$ correlated $\mathcal{B}$-field: $\mathcal{B}^{\mathcal{E}}$ (to simulate $\vec{v}\times\vec{\mathcal{E}}$/geometric phase/leakage current effects)
Electric Fields
- Non-Reversing $\mathcal{E}$-Field: $\mathcal{E}^{\rm nr}$
- $\mathcal{E}$-Field Ground Offset
Laser Detunings
- Detuning of the Prep/Read Lasers: $\Delta_{\rm prep}$, $\Delta_{\rm read}$
- $\tilde{\mathcal{P}}$ correlated Detuning: $\Delta^{\mathcal{P}}$
- $\tilde{\mathcal{N}}$ correlated Detunings: $\Delta^{\mathcal{N}}$, $\Delta\Delta^{\mathcal{N}}$
Laser Pointings along $\hat{x}$
- Change in Pointing of Prep/Read Lasers
- Readout laser $\hat{X}/\hat{Y}$ dependent pointing
- $\tilde{\mathcal{N}}$ correlated laser pointing
- $\tilde{\mathcal{N}}$ and $\hat{X}/\hat{Y}$ dependent laser pointing
Laser Powers
- Power of Prep/Read Lasers: $P_{\rm prep}$, $P_{\rm read}$
- $\tilde{\mathcal{N}}\tilde{\mathcal{E}}$ correlated power, $P^{\mathcal{NE}}$ (simulating $\Omega_r^{\mathcal{NE}}$)
- $\tilde{\mathcal{N}}$ correlated power, $P^{\mathcal{N}}$
- $\hat{X}/\hat{Y}$ dependent Readout laser power
Laser Polarization
- Preparation Laser Ellipticity
Molecular Beam Clipping
- Molecule Beam Clipping along the $\hat{y}$ and $\hat{z}$ (changes $\langle v_y\rangle$,$\langle v_z\rangle$,$\langle y\rangle$,$\langle z\rangle$ for molecule ensemble)
Category II Parameters
Experiment Timing
- $\hat{X}/\hat{Y}$ Polarization Switching Rate
- Number of Molecule Pulse Averages contributing to an Experiment State
Analysis
- Signal size cuts, Asymmetry magnitude cuts, Contrast cuts
- Difference between two PMT detectors (checking spatial fluorescence region dependence)
- Variation with time within molecule pulse (serves to check v_x dependence)
- Variation with time within polarization switching cycle
- Variation with time throughout the full dataset (autocorrelation)
- Search for correlations with all ϕ, $\mathcal{C}$, and S switch-parity components
- Search for correlations with auxiliary measurements of $\mathcal{B}$-fields, laser powers, and vacuum pressure
- 3 individuals performed independent analyses of the data

TABLE S1. **Parameters varied in the search for systematic errors.** Category I: Parameters that were varied far from their values under normal conditions of the experiment. For each of these parameters direct measurements or limits were placed on possible systematic errors that could couple linearly to each by the method described in the main text. Category II: Parameters for which all values are considered consistent with normal conditions of the experiment. Although direct limits on systematic errors cannot be derived, these served as checks for the presence of unanticipated systematic errors.

by $|H,\tilde{\mathcal{N}},M=+1\rangle\leftrightarrow|C,\tilde{\mathcal{P}},M=0\rangle\leftrightarrow|H,\tilde{\mathcal{N}},M=-1\rangle$. Such a Λ system has a dark eigenstate (a state that has zero excited state $|C,\tilde{\mathcal{P}},M=0\rangle$ amplitude) in the limit of $\delta=0$, but for $\delta\neq 0$, all eigenstates have nonzero excited state amplitude. In the limit of

small $\delta/\Omega_r \ll 1$ (in our case, $\delta/\Omega_r \sim 10^{-3}$), the introduction of the magnetic field mixes the bright and dark states with amplitudes proportional to δ/Ω_r. The bright state amplitude acquires an AC Stark shift and results in a change in the measured phase that is correlated with the magnetic field direction,

$$\phi^{\mathcal{B}}_{\mathrm{AC}}(\Delta,\Omega_r) = \alpha^{\mathcal{B}}\Delta^2 + \beta^{\mathcal{B}}\Omega_r, \tag{S1}$$

where $\alpha^{\mathcal{B}}$ and $\beta^{\mathcal{B}}$ are proportional to $|\mathcal{B}_z|$ and depend on the spatial profile of the laser. This model was verified and these coefficients were measured directly from $\phi^{\mathcal{B}}$ by varying Δ and Ω_r with AOMs.

The coupling of the $\Delta^{\mathcal{N}\mathcal{E}}$ and $\Omega_r^{\mathcal{N}\mathcal{E}}$ to this $\tilde{\mathcal{B}}$-odd AC Stark shift-induced phase leads to contributions to $\phi^{\mathcal{N}\mathcal{E}\mathcal{B}}$:

$$\phi^{\mathcal{N}\mathcal{E}\mathcal{B}} = 2\alpha^{\mathcal{B}}\Delta\Delta^{\mathcal{N}\mathcal{E}} + \beta^{\mathcal{B}}\Omega_r^{\mathcal{N}\mathcal{E}}. \tag{S2}$$

This phase is dominated by the $\beta^{\mathcal{B}}\Omega_r^{\mathcal{N}\mathcal{E}}$ term since we operate the experiment on resonance, $\Delta \approx 0$; this was verified by observing that $\phi^{\mathcal{N}\mathcal{E}\mathcal{B}}$ reversed sign with $\hat{k}\cdot\hat{z}$ (since $\Omega_r^{\mathcal{N}\mathcal{E}} \propto \hat{k}\cdot\hat{z}$). We used this effect to our advantage to measure the value of $\Omega_r^{\mathcal{N}\mathcal{E}} = \phi^{\mathcal{N}\mathcal{E}\mathcal{B}}/\beta^{\mathcal{B}}$ in our system. We measured $\phi^{\mathcal{N}\mathcal{E}\mathcal{B}}$ from our EDM dataset, and we measured $\beta^{\mathcal{B}} = \partial\phi^{\mathcal{N}\mathcal{E}\mathcal{B}}/\partial\Omega^{\mathcal{N}\mathcal{E}}$ by intentionally correlating the laser power of the state preparation and read-out lasers with $\tilde{\mathcal{N}}\tilde{\mathcal{E}}$ using AOMs.

The $\mathcal{E}^{\mathrm{nr}}$ and $\Omega_r^{\mathcal{N}\mathcal{E}}$ systematics, which result from AC Stark shift induced phases, were sensitive to the spatial intensity profile and polarization gradients in the prep and readout lasers. A sharper edge to the laser intensity profile reduces the size of the region where the AC stark shift phase accumulates, therefore reducing the systematic slopes proportional to α and β. The dependence on the spatial intensity profile was confirmed by clipping our Gaussian laser beam profile with a razor edge. This data agreed with numerical simulations of the Schrödinger equation under varying spatial intensity profiles. To vary the polarization gradients, an optical chopping wheel was added on the state preparation laser beam, reducing the time averaged energy deposited in the field plates and hence also the thermally induced birefringence. As expected, the slope of the $\mathcal{E}^{\mathrm{nr}}$ systematic was also reduced by half.

The two $\tilde{\mathcal{N}}$ states in which we perform our EDM measurement have magnetic moments differing by about 0.1 percent[12]. This difference is proportional to $|\mathcal{E}_z|$ and is the main contribution to $\phi^{\mathcal{N}\mathcal{B}}$. Therefore, any effect coupling to the magnetic moment to systematically shift $\phi^{\mathcal{E}}$ will also produce a 1000-times smaller shift in $\phi^{\mathcal{N}\mathcal{E}}$. We verified this by intentionally correlating a 1.4 mG component of $\mathcal{B}_z$ with $\tilde{\mathcal{E}}$, resulting in a large offset of $\phi^{\mathcal{E}}$ and a 1000-times smaller offset of $\phi^{\mathcal{N}\mathcal{E}}$, as expected. Although $\phi^{\mathcal{E}}$ shifts caused by leakage current, $\vec{v}\times\vec{\mathcal{E}}$, and geometric phase effects were observed in past experiments[4], we expect to be immune to such effects at our current level of sensitivity[10]. Indeed, the measured $\phi^{\mathcal{E}}$ was consistent with zero for our reported data set. The mean and uncertainty of $\phi^{\mathcal{E}}$, divided by the measured suppression factor, is included in our $\phi^{\mathcal{N}\mathcal{E}}$ systematic error budget (see Table 1).

Data was stored and analyzed as a function of time after ablation and time within a polarization switch state. Due to the 10 percent longitudinal velocity dispersion of our molecule beam, the arrival time at our detectors is correlated with different longitudinal velocity classes, and therefore different precession times τ. We did not see any variation in the measured phases $\phi^{\mathcal{E}}$ or $\phi^{\mathcal{N}\mathcal{E}}$ as a function of time after ablation.

Outlook

It is possible to further reduce this experiment's statistical and systematic uncertainty. In a separate apparatus we have demonstrated that electrostatic molecule focusing and EDM state preparation via Stimulated Raman Adiabatic Passage can combine to increase our fluorescence signal by a factor of ~ 100. Also, a thermochemical beam source may increase our molecule flux by a factor of ~ 10. The combined signal increase may reduce our statistical uncertainty by a factor of $\gtrsim 10$. The dominant AC Stark shift systematic errors can be further suppressed by implementing electric field plates with improved thermal and optical properties.

References

1. P. G. H. Sandars, The electric dipole moment of an atom. *Phys. Lett.* **14**, 194–196 (1965). doi:10.1016/0031-9163(65)90583-4

2. I. B. Khriplovich, S. K. Lamoreaux, *CP Violation Without Strangeness* (Springer, New York, 1997).

3. E. D. Commins, D. DeMille, in *Lepton Dipole Moments*, B. L. Roberts, W. J. Marciano, Eds. (World Scientific, Singapore, 2010), chap. 14, pp. 519–581.

4. B. Regan, E. Commins, C. Schmidt, D. DeMille, New limit on the electron electric dipole moment. *Phys. Rev. Lett.* **88**, 071805 (2002). doi:10.1103/PhysRevLett.88.071805

5. J. J. Hudson, D. M. Kara, I. J. Smallman, B. E. Sauer, M. R. Tarbutt, E. A. Hinds, Improved measurement of the shape of the electron. *Nature* **473**, 493–496 (2011). doi:10.1038/nature10104 Medline

6. D. M. Kara, I. J. Smallman, J. J. Hudson, B. E. Sauer, M. R. Tarbutt, E. A. Hinds, Measurement of the electron's electric dipole moment using YbF molecules: Methods and data analysis. *New J. Phys.* **14**, 103051 (2012). doi:10.1088/1367-2630/14/10/103051

7. M. A. Player, P. G. H. Sandars, An experiment to search for an electric dipole moment in the $^3P_2$ metastable state of xenon. *J. Phys. B* **3**, 1620–1635 (1970). doi:10.1088/0022-3700/3/12/007

8. L. V. Skripnikov, A. N. Petrov, A. V. Titov, Theoretical study of ThO for the electron electric dipole moment search. *J. Chem. Phys.* **139**, 221103 (2013). doi:10.1063/1.4843955

9. E. R. Meyer, J. L. Bohn, Prospects for an electron electric-dipole moment search in metastable ThO and ThF^+. *Phys. Rev. A* **78**, 010502 (2008). doi:10.1103/PhysRevA.78.010502

10. A. C. Vutha, W. C. Campbell, Y. V. Gurevich, N. R. Hutzler, M. Parsons, D. Patterson, E. Petrik, B. Spaun, J. M. Doyle, G. Gabrielse, D. DeMille, Search for the electric dipole moment of the electron with thorium monoxide. *J. Phys. B* **43**, 074007 (2010). doi:10.1088/0953-4075/43/7/074007

11. A. C. Vutha, B. Spaun, Y. V. Gurevich, N. R. Hutzler, E. Kirilov, J. M. Doyle, G. Gabrielse, D. DeMille, Magnetic and electric dipole moments of the $H^3\Delta_1$ state in ThO. *Phys. Rev. A* **84**, 034502 (2011). doi:10.1103/PhysRevA.84.034502

12. S. Bickman, P. Hamilton, Y. Jiang, D. DeMille, Preparation and detection of states with simultaneous spin alignment and selectable molecular orientation in PbO. *Phys. Rev. A* **80**, 023418 (2009). doi:10.1103/PhysRevA.80.023418

13. S. Eckel, P. Hamilton, E. Kirilov, H. W. Smith, D. DeMille, Search for the electron electric dipole moment using Ω-doublet levels in PbO. *Phys. Rev. A* **87**, 052130 (2013). doi:10.1103/PhysRevA.87.052130

14. W. C. Campbell *et al*., EPJ Web of Conferences 57, 02004 (2013).

15. E. Kirilov, W. C. Campbell, J. M. Doyle, G. Gabrielse, Y. V. Gurevich, P. W. Hess, N. R. Hutzler, B. R. O'Leary, E. Petrik, B. Spaun, A. C. Vutha, D. DeMille, Shot-noise-limited spin measurements in a pulsed molecular beam. *Phys. Rev. A* **88**, 013844 (2013). doi:10.1103/PhysRevA.88.013844

16. S. E. Maxwell, N. Brahms, R. deCarvalho, D. R. Glenn, J. S. Helton, S. V. Nguyen, D. Patterson, J. Petricka, D. DeMille, J. M. Doyle, High-flux beam source for cold, slow atoms or molecules. *Phys. Rev. Lett.* **95**, 173201 (2005). doi:10.1103/PhysRevLett.95.173201 Medline

17. N. R. Hutzler, M. F. Parsons, Y. V. Gurevich, P. W. Hess, E. Petrik, B. Spaun, A. C. Vutha, D. DeMille, G. Gabrielse, J. M. Doyle, A cryogenic beam of refractory, chemically reactive molecules with expansion cooling. *Phys. Chem. Chem. Phys.* **13**, 18976 (2011). doi:10.1039/c1cp20901a Medline

18. N. R. Hutzler, H.-I. Lu, J. M. Doyle, The buffer gas beam: An intense, cold, and slow source for atoms and molecules. *Chem. Rev.* **112**, 4803–4827 (2012). doi:10.1021/cr200362u Medline

19. H. R. Gray, R. M. Whitley, C. R. Stroud Jr., Coherent trapping of atomic populations. *Opt. Lett.* **3**, 218–220 (1978). doi:10.1364/OL.3.000218 Medline

20. G. J. Feldman, R. D. Cousins, Unified approach to the classical statistical analysis of small signals. *Phys. Rev. D* **57**, 3873–3889 (1998). doi:10.1103/PhysRevD.57.3873

21. J. H. Curtiss, On the distribution of the quotient of two chance variables. *Ann. Math. Stat.* **12**, 409–421 (1941). doi:10.1214/aoms/1177731679

22. S. Eisenbach, H. Lotem, SPIE 8th Meeting on Optical Engineering in Israel 1972 (1992).

23. H. G. Berry, G. Gabrielse, A. E. Livingston, Measurement of the Stokes parameters of light. *Appl. Opt.* **16**, 3200–3205 (1977). doi:10.1364/AO.16.003200 Medline

24. M. G. Kozlov, L. N. Labzowsky, Parity violation effects in diatomics. *J. Phys. At. Mol. Opt. Phys.* **28**, 1933–1961 (1995). doi:10.1088/0953-4075/28/10/008

25. V. A. Dzuba, V. V. Flambaum, C. Harabati, Relations between matrix elements of different weak interactions and interpretation of the parity-nonconserving and electron electric-dipole-moment measurements in atoms and molecules. *Phys. Rev. A* **84**, 052108 (2011). doi:10.1103/PhysRevA.84.052108

26. W. C. Griffith, M. D. Swallows, T. H. Loftus, M. V. Romalis, B. R. Heckel, E. N. Fortson, Improved limit on the permanent electric dipole moment of ^{199}Hg. *Phys. Rev. Lett.* **102**, 101601 (2009). doi:10.1103/PhysRevLett.102.101601 Medline

27. S. Barr, A review of CP violation in atoms. *Int. J. Mod. Phys. A* **08**, 209–236 (1993). doi:10.1142/S0217751X93000096

28. M. Pospelov, A. Ritz, Electric dipole moments as probes of new physics. *Ann. Phys.* **318**, 119–169 (2005). doi:10.1016/j.aop.2005.04.002

29. J. Engel, M. J. Ramsey-Musolf, U. van Kolck, Electric dipole moments of nucleons, nuclei, and atoms: The Standard Model and beyond. *Prog. Part. Nucl. Phys.* **71**, 21–74 (2013). doi:10.1016/j.ppnp.2013.03.003

30. N. Fortson, P. Sandars, S. Barr, The search for a permanent electric dipole moment. *Phys. Today* **56**, 33 (2003). doi:10.1063/1.1595052

31. W. Bernreuther, M. Suzuki, The electric dipole moment of the electron. *Rev. Mod. Phys.* **63**, 313–340 (1991). doi:10.1103/RevModPhys.63.313

32. R. A. Patten, Michelson interferometer as a remote gauge. *Appl. Opt.* **10**, 2717–2721 (1971). doi:10.1364/AO.10.002717 Medline

33. J. Hall, L.-S. Ma, M. Taubman, B. Tiemann, F.-L. Hong, O. Pfister, Jun Ye, Stabilization and frequency measurement of the I_2-stabilized Nd:YAG laser. *IEEE Trans. Instrum. Meas.* **48**, 583–586 (1999). doi:10.1109/19.769663

34. G. Edvinsson, A. Bornstedt, P. Nylén, *Ark. Phys.* **38**, 193 (1968).

35. G. Edvinsson, A. Lagerqvist, Two new band systems in ThO. *Phys. Scr.* **41**, 316–320 (1990). doi:10.1088/0031-8949/41/3/004

36. J. Paulovič, T. Nakajima, K. Hirao, R. Lindh, P. A. Malmqvist, Relativistic and correlated calculations on the ground and excited states of ThO. *J. Chem. Phys.* **119**, 798 (2003). doi:10.1063/1.1578053